Autonomous Control and Parameter Optimization for Electrolytic Aluminum Loads Participating in Primary Frequency Regulation Ancillary Services

Siyang Liao[a], Shanquan Pi[a], Jian Xu[a*], Lingfang Li[b], Deping Ke[a], Yuanzhang Sun[a]

[a]*Hubei Engineering and Technology Research Center for AC/DC Intelligent Distribution Network, School of Electrical Engineering and Automation, Wuhan University, Wuhan 430072, China*

[b]*Power Grid Planning and Construction Center of Yunnan Power Grid Co., Ltd, Kunming 650000, China*

***Correspondence**: Jian Xu, School of Electrical Engineering and Automation, Wuhan University, Wuhan 430072, China. Email: xujian@whu.edu.cn*

Abstract

Electrolytic aluminum (EAL) loads, with their large capacities and fast active power regulation capability, are promising providers of primary frequency regulation (PFR) ancillary services. However, their practical participation remains limited by the incompatibility between existing industrial control systems and PFR requirements, as well as by production constraints. This paper proposes an autonomous PFR control and parameter optimization framework that accounts for net economic benefit and production safety. A local frequency feedback loop is integrated into the existing industrial current control system, enabling EAL loads to respond autonomously to frequency deviations. An electrical, thermal, and material coupled dynamic model is established to characterize key production states, and production safety constraints are quantitatively mapped into energy boundaries applicable to PFR control. Based on these boundaries, a multi-objective optimization model determines the frequency deadband and droop coefficient by considering net economic benefit and production risk. The resulting Pareto optimal parameter set enables aluminum smelters to determine PFR control parameters according to their operating requirements and risk preferences. Case studies verify that the proposed framework enables autonomous and economically beneficial participation in PFR ancillary services while maintaining production safety.

Keywords: ancillary service, demand response, electrolytic aluminum load, multiphysics modeling, primary frequency regulation

1. Introduction

The large-scale integration of renewable energy has progressively reduced power system inertia and displaced part of the primary frequency regulation (PFR) capability traditionally provided by synchronous generators, increasing the demand for alternative frequency regulation resources [1, 2]. Compared with dedicated energy storage, demand-side resources can provide frequency regulation by exploiting the inherent flexibility of existing electrical loads, thereby avoiding additional energy-storage investment and offering considerable potential for large-scale deployment. Among various demand-side resources, energy-intensive industrial loads are particularly attractive because of their large power capacities, continuous operating characteristics, and substantial regulation potential. In China, for example, the flexible regulation potential of energy-intensive industrial loads is estimated at approximately 108 GW, corresponding to nearly 19.3% of the power supply-demand imbalance [3]. These characteristics make energy-intensive industrial loads promising large-scale providers of PFR ancillary services.

Among energy-intensive industries, including steel, cement, and chemical production, electrolytic aluminum (EAL) plants exhibit particularly strong potential for PFR because of their large load capacities, fast power regulation capability, and high control precision [4]. In 2025, the electricity consumption of China’s EAL industry accounted for approximately 5.86% of the national electricity demand [5, 6], with an even higher concentration in regions with a high concentration of new energy resources. For example, the annual electricity consumption of the EAL industry in Yunnan Province is projected to exceed 60 TWh, accounting for nearly 25% of the province's total electricity consumption [7]. A single aluminum smelter typically has a load capacity of 300–800 MW [8], while current regulation based on saturable reactor enables millisecond-scale power adjustment over a range of approximately 8%, meeting the fast-response requirements of PFR. Meanwhile, recent ancillary service market reforms have increasingly enabled eligible energy-intensive industrial consumers to participate in PFR and receive compensation for their regulation services. Therefore, EAL plants possess both the technical capability and the economic incentive to act as large-scale providers of PFR ancillary services.

However, translating the regulation potential of EAL loads into practically deployable PFR ancillary services remains challenging in two key respects. First, PFR requires participating resources to respond autonomously to local frequency deviations following a disturbance, whereas existing EAL control systems are primarily designed for production-oriented power or current regulation and therefore lack a local autonomous control framework tailored to PFR. Second, ancillary service compensation is typically linked to the actual regulation energy delivered or the achieved regulation performance. Consequently, key control parameters, such as the frequency deadband and droop coefficient, determine not only the frequency regulation response and potential economic returns of EAL loads, but also the resulting power fluctuations and their impacts on the safe operation of the electrolysis process. Therefore, enabling EAL loads to participate effectively in PFR ancillary services requires both an autonomous local response mechanism and a optimization method for configuring PFR control parameters under production safety constraints, so as to balance frequency regulation benefits against the associated impacts on production operation.

Existing studies have long explored the participation of EAL loads in PFR. Early research mainly focused on regulating EAL power through external control commands. For example, [9] adjusted generator excitation voltage in an isolated power system to modify the load bus voltage and active power, thereby improving the system frequency response following disturbances. Reference [10] further coordinated the adjustment of generator excitation voltage and the voltage drop across the saturable reactor to exploit additional regulation capability. Reference [11] extended this concept to large power systems and developed an optimization method for EAL control commands subject to frequency constraints. These studies demonstrated the technical potential of EAL loads for frequency regulation. However, they all rely on regulation commands issued by the power grid and therefore represent externally commanded power regulation rather than autonomous response to local frequency deviations. Since EAL loads normally operate at nearly constant power, their active power is inherently insensitive to frequency variations. Enabling EAL loads to provide PFR therefore requires the introduction of frequency measurement and feedback into the existing production control system, so that a local autonomous PFR mechanism can be established while minimizing modifications to the original industrial control architecture.

However, equipping EAL loads with autonomous PFR capability alone is insufficient to support their effective participation in PFR ancillary services. Appropriate configuration of key control parameters is equally important. The frequency deadband and droop coefficient directly determine the magnitude and duration of the power response under different frequency deviations and consequently affect both the regulation energy delivered and the resulting ancillary service revenue. Under the relevant ancillary service mechanism of China Southern Power Grid, loads participating in PFR can receive compensation according to their actual regulation contribution. More aggressive parameter settings may therefore increase the potential economic return from frequency regulation. On the other hand, EAL production is normally maintained around a relatively stable power operating point, and frequent or large power variations can disturb the thermal and material balances of the electrolysis process. Therefore, PFR parameter design should not simply pursue a larger regulation response, but should coordinate the economic benefit of ancillary service participation with the resulting impact on production operation.

In addition, the optimization of PFR parameters must satisfy production safety constraints, and translating these production constraints into regulation boundaries that can be directly incorporated into parameter optimization remains a major challenge. Some existing studies determine the available regulation capacity mainly from electrical equipment limits, such as the operating range of the saturable reactor [12]. Such constraints characterize the instantaneous power regulation capability but cannot adequately capture the cumulative effects of energy deviations during sustained frequency regulation. EAL production requires the thermal and material balances of the electrolysis process to remain within relatively narrow ranges. Sustained power deviations can create an energy imbalance, which may further alter the electrolyte temperature and alumina concentration and, in severe cases, lead to operational failures such as cell freezing and substantial economic losses. However, these production safety limits arise from highly coupled thermodynamic and electrochemical processes [13] and therefore cannot be directly expressed as the power or energy constraints required for PFR control. Although several studies have investigated the effects of energy variations on electrolyte temperature and alumina concentration [14, 15], a quantitative mapping from production state constraints to PFR regulation energy limits has not yet been established. Consequently, existing models cannot directly support the safe optimization of PFR control parameters.

To address the above challenges, this paper proposes an autonomous control and parameter optimization framework for EAL participation in PFR ancillary services. The proposed framework enables EAL loads to respond autonomously to local frequency deviations while satisfying production safety constraints and coordinates ancillary service revenue with the resulting impacts on production operation. The main contributions are summarized as follows.

(1) An autonomous PFR framework compatible with existing industrial control systems is proposed for EAL loads. Frequency measurement and feedback are incorporated into the existing current control system, together with a frequency monitoring unit and a programmable logic controller. This enables EAL loads to autonomously regulate their power according to locally measured frequency deviations and to configure the corresponding PFR control parameters according to the current production state. By retaining the original production control functions and requiring only limited modifications to the existing control system, the proposed framework enables rapid local PFR response and provides a practical control solution for industrial loads participating in PFR ancillary services.

(2) A quantitative mapping method from production safety constraints to safe PFR operating boundaries is developed. Based on an electrical, thermal, and material coupled dynamic model of the aluminum electrolysis cell, the dynamic variations in key production states, including electrolyte temperature and alumina concentration, during power regulation are characterized. The associated thermodynamic and electrochemical safety constraints are then transformed into energy boundaries that can be directly incorporated into PFR control. This method overcomes the limitations of evaluating PFR capability solely from the regulation ranges of electrical equipment and provides quantitative constraints for the safe configuration of PFR control parameters.

(3) A multi-objective optimization method for PFR parameters is proposed to coordinate ancillary service revenue and production risk. The frequency deadband and droop coefficient are optimized while satisfying the derived production safety boundaries, with the objectives of maximizing PFR ancillary service revenue and minimizing production risk caused by frequency regulation. The resulting Pareto optimal parameter set enables aluminum smelters to select appropriate PFR parameters according to their operating requirements and risk preferences, thereby achieving a balanced tradeoff between economic benefits and production risk while maintaining production safety.

The remainder of this paper is organized as follows. Section II characterizes the production process and the electrical properties of EAL loads, followed by the derivation of multiphysics-based regulation boundaries. Section III establishes the autonomous PFR control framework and formulates the parameter optimization model. Section IV provides simulation results and performance evaluations to validate the proposed strategy. Finally, Section V concludes the paper.

2. Multiphysics modeling and regulation boundaries of EAL for PFR

2.1. Production process of EAL

The production of EAL generally follows the Hall-Héroult process, in which alumina is dissolved in molten cryolite and reduced to aluminum under high-temperature conditions.

Electricity is the primary energy source in production process, and EAL is generally designed to operate at constant power. Variations in power directly affect output and indirectly impact production safety and efficiency. Safe and efficient operation relies on two conditions: thermal balance and material balance[16].

The key parameter of thermal balance is the bath temperature. Approximately 50% of the electricity input is converted into heat, maintaining the temperature at around 960 °C to ensure the dissolution of alumina and stable electrochemical reactions. Excessive temperature reduces current efficiency and production profit, whereas an excessively low temperature may solidify the electrolyte, leading to operational instability and severe production losses. Industrially, aluminum smelters use the current control system to keep the power and the temperature constant.

The key parameter of material balance is the alumina concentration. Alumina is an important raw material for the production of aluminum. About two tons of alumina are consumed to produce one ton of aluminum. Modern electrolytic cells are equipped with automatic feeders that maintain the alumina concentration within the range of 1.5-2.5wt.% [17] through timing feed control, adaptive concentration control, etc. A high concentration tends to cause alumina precipitation at the cell bottom, decreasing current efficiency and increasing cost. Conversely, a low concentration may trigger anode effects, leading to a rapid rise in cell voltage, excessive power consumption, and, in extreme cases, endangering cell integrity [18]. Under normal operating conditions, the electrolysis current remains close to rated value, and the alumina feed and consumption maintain a dynamic equilibrium, keeping the alumina concentration stable.

In essence, the electrolytic process inherently couples multiple physical domains—electrical, thermal, and material. During normal production, the electrolytic cell runs at constant power to maintain the thermal balance and material balance, as well as stable aluminum production. However, during PFR, power fluctuations disturb these balances, causing deviations in bath temperature and alumina concentration. Such deviations reduce production efficiency and, in severe cases, may compromise operational safety.

Therefore, it is essential to model the power–temperature and power–alumina concentration relationships, thereby transforming the non-electrical constraints related to process safety into electrical constraints applicable to frequency regulation analysis.

2.2. Electrical characteristics and control characteristics of EAL

The EAL load is a typical low-voltage high-current load. The AC voltage is stepped down by the on-load tap changing (OLTC) transformers and rectified by the saturable reactors-diodes, and then converted into the lower DC voltage. The DC part is the main electricity consumption part, which is generally expressed as a series connection of a back electromotive force and an equivalent resistance.

The DC voltage V_d can be calculated by [10]:

$$V_d = 1.35(V_{AH} / k - V_{sr}) \tag{1}$$

where V_{AH} is the voltage on the high-voltage side of the load bus, k is the ratio of the OLTC transformer, and V_{sr} is the voltage drop of the saturable reactor.

The relationship between load power, DC current and DC voltage is:

$$P_d = I_d V_d \tag{2}$$

$$I_d = \frac{V_d - E}{R} \tag{3}$$

where I_d is the DC current, R is the equivalent resistance, and E is the back electromotive force.

According to (1)-(3), load power can be adjusted by adjusting either the ratio of the OLTC transformer or the voltage drop of the saturable reactor. The characteristics of the two adjustment methods are summarized in Table 1.

Since PFR requires fast and continuous power regulation, this paper considers only the method of adjusting the saturable reactor for power regulation.

The production control system of EAL includes a current closed-loop control system that maintains current constant. The control block diagram of the current control system is shown in Fig. 1.

The current control system measures the DC current of the electrolytic cell, and compare it the reference current. The resulting error is processed through a delay block and a PI controller to determine the voltage drop of the saturable reactor. This voltage adjustment modifies the input DC voltage, thereby regulating the DC current until it matches the reference value.

Therefore, power regulation through the saturable reactor can be achieved simply by adjusting the DC reference current.

The saturable reactor usually operates at 20~40V, and its adjustment range is generally 0~70V. By changing the voltage drop of the saturable reactor, the load power can be adjusted upward or downward.

The variation range of the voltage drop of the saturable reactor is [$\Delta V_{sr,down}$, $\Delta V_{sr,up}$]

Table 1
Adjustment methods and characteristics of EAL load [12]

adjustment variables	**response speed**	**discrete/ continuous**	**adjustable range**
ratio of the OLTC transformer	about 6~7 seconds per tap position	discrete	about 3% P_N per tap position
voltage drop of the saturable reactor	millisecond-level	continuous	about ±7% P_N

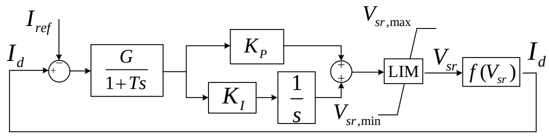

Fig. 1 Control block diagram of the current control system.

Combining (1)-(3) the adjustable range of the DC current can be determined as [$\Delta I_{ref,own}$, $\Delta I_{ref,up}$].

$$\Delta I_{ref,up} = \frac{-1.35\Delta V_{sr,down}}{R} \tag{4}$$

$$\Delta I_{ref,down} = \frac{-1.35\Delta V_{sr,up}}{R} \tag{5}$$

2.3. Electrical regulation boundaries based on multiphysics constraints

Based on the above analysis, power fluctuations during PFR perturb the critical thermal and material balances of the electrolytic cell, thereby threatening production safety. To ensure operational stability, these thermal and material balance requirements are modeled and equivalently transformed into electrical regulation boundary constraints.

(1) thermal balance constraints

The thermal power balance mechanism of the electrolytic cell can be formulated as follows [19].

$$\begin{aligned} &(V_d - V_{RE}) \times I_d = \\ &h(T_b - T_L)A_{wall} + h(T_b - T_L)A_{top} + h(T_b - T_L)A_{bottom} \end{aligned} \tag{6}$$

where V_{RE} is the reaction voltage; h is the heat transfer coefficient between the electrolyte and the sidewalls, top, and bottom surfaces; (T_b-T_L) represents the temperature difference between the electrolyte and each solid interface; A is the contact area of the electrolyte–solid interfaces.

The left-hand side of the equation quantifies the heat generation, which is defined as the total electricity supplied to the cell less the power consumed by the electrochemical reaction. The right-hand side represents the heat dissipation, specifically the power transferred from the electrolyte to the internal solid interfaces.

This equation describes the energy conversion and transfer within the cell. A portion of the electricity input drives the electrochemical reaction, while the remainder is converted into thermal energy. This heat is subsequently transferred away from the electrolyte to solid components and is ultimately dissipated into the ambient environment.

During PFR, variations in the input current induce corresponding changes in the input power, which in turn disturb the power balance of the electrolytic cell and cause the bath temperature to deviate from nominal value.

The reaction voltage is determined solely by the current efficiency and is independent of the electrolysis current. Empirical observations indicate that for every 10 °C decrease in bath temperature, the current efficiency increases by approximately 1~1.5% [20]. Considering the short timescale of PFR and the relatively small temperature fluctuation involved, the reaction voltage can be reasonably assumed to remain constant before and after the PFR.

Accordingly, when variations in heat dissipation are neglected, the unbalanced power of the electrolytic cell can be expressed as follows.

$$\Delta E_0(t) = \left(V_0 - V_{re}\right) I_0 - \left(V_1(t) - V_{re}\right) I_1(t) \tag{7}$$

where V_1, I_1 represent the adjusted voltage and current, while V_0, I_0 correspond to initial values.

However, when the bath temperature varies, the convective heat transfer between the electrolyte and the solid interfaces also changes. These variations in convective heat flow partially offset the overall power imbalance within the cell. Owing to the large thermal inertia of the cell bottom, it is reasonable to assume that the heat dissipation through the bottom remains constant during the regulation process.

Accordingly, the actual unbalanced power at time t is defined as the change in input power available for heat dissipation minus the corresponding change in convective heat transfer. This unbalanced power results in temporal variations in the bath temperature.

$$\begin{gathered}\Delta E(t) = \Delta E_0(t) - \\ \left[E_{wall,0} + E_{top,0} - hA_{wall+top}\left(T_b(t) - T_L\right)\right]\end{gathered} \tag{8}$$

where $E_{wall,0}$ and $E_{top,0}$ are the heat dissipation of the sidewalls and top before PFR, respectively.

Based on this relationship, the dynamic behavior of the bath temperature can be described by a first-order differential equation.

$$\begin{gathered}cm\frac{dT_b(t)}{dt} = \Delta E(t) = \Delta E_0(t) - \\ \left[\alpha E_0 - hA_{wall+top}(T_b(t) - T_L)\right]\end{gathered} \tag{9}$$

where c is the specific heat capacity of the electrolyte and m is the mass of the electrolyte, E_0 is the total heat dissipation before PFR, α denotes the fraction of heat dissipated occurring through the top and sidewalls of the electrolytic cell. In practice, heat dissipation from these surfaces typically account for approximately 85–90% of the total heat dissipation.

Discretizing this differential equation using the explicit finite difference method yields the bath temperature at each time step:

$$\begin{gathered}cm\left[T(t+1) - T(t)\right] = \\ \Delta E_0(t)\Delta t - \left[\alpha E_0 - hA_{wall+top}\left(T(t) - T_L\right)\right]\Delta t\end{gathered} \tag{10}$$

where Δt is the time step.

Therefore, the temperature constraint can be expressed as:

$$T_{\min} \le T(t) \le T_{\max} \quad \forall t \in \left[0, t_{end}\right] \tag{11}$$

Equations (10) and (11) link the power imbalance during PFR to the thermal state of the electrolyte. Since the bath temperature depends on the power deviation ΔE_0(t), the limits defined in (11) effectively constrain the allowable range of the power imbalance. Consequently, the non-electrical thermal balance constraints define the boundaries for the PFR regulation capacity, ensuring that the electrolytic cell remains within its safe operational margin.

(2) material balance constraints

During the production process, the alumina content within the electrolytic cell can be expressed as,

$$M = M_0 + M_{INV} - M_{CONS} \tag{12}$$

where M is the current alumina content, M_0 is the initial alumina content in the cell, which can be recorded as a constant, M_{INV} represents the alumina feed, M_{CONS} denotes the alumina consumption.

The feeding rate of the electrolytic cell is assumed constant over a short time interval; therefore, the feed amount can be formulated as a function of time:

$$M_{INV} = k_1 t \tag{13}$$

where k_1 is the feeding rate (kg/h).

Since alumina consumption is proportional to the output of EAL, it can be expressed as

$$M_{CONS} = k_2 M_{AL} \tag{14}$$

where k_2 is the alumina consumption per ton of aluminum produced, and M_{AL} denotes the aluminum output.

According to [21], the aluminum production is related to the electrolysis current as

$$M_{AL} = 0.3356 I t \eta \tag{15}$$

where I is the current intensity, t is the electrolysis time, and η is the current efficiency.

Substituting (13)–(15) into (12), the dynamic expression of alumina content can be obtained as:

$$M(t) = M_0 + k_1 t - k_2 \cdot 0.3356 I t \eta \tag{16}$$

The system operates in the overfeeding state when k_1-k_2·0.3356$I\eta$≥0, and in the under-feeding state when k_1-k_2·0.3356$I\eta$≤0. During normal operation, the production control system of EAL is designed to alternate between overfeeding and underfeeding conditions in order to maintain the alumina concentration within a narrow operating range..

When EAL participates in PFR, the feeding rate remains unchanged. As the input electricity decreases, aluminum production is correspondingly reduced, which ultimately affects the alumina concentration within the electrolytic cell.

Accordingly, the alumina content in the electrolytic cell under both normal production and PFR conditions can be expressed as follows:

$$M_N = k_1 t - k_2 \cdot 0.3356 I_N t\eta + M_0 \tag{17}$$

$$M_F = k_1 t - k_2 \cdot 0.3356 I_f t\eta + M_0 \tag{18}$$

where I_N is the rated value of the electrolysis current, and I_f is the current when participating in PFR.

Since the alumina concentration generally maintained within the range of 1.5-2.5wt.%, it is reasonable to assume that, during PFR, the alumina content in the cell exhibits a small deviation compared with normal operation and must satisfy the following constraint:

$$L_{down} \le M_F / M_N \le L_{up} \tag{19}$$

where L_{up} and L_{down} denote the upper and lower bounds of the deviation, respectively.

Therefore, to ensure material balance within the electrolytic cell during PFR, the electrolysis current must satisfy the following constraint:

$$1 - \frac{(L_{up}-1)M_N}{0.3356 k_2 I_N \eta t} \le \frac{\int I_f \mathrm{d}t}{\int I_N \mathrm{d}t} \le 1 - \frac{(L_{down}-1)M_N}{0.3356 k_2 I_N \eta t} \tag{20}$$

3. Autonomous PFR control framework and parameter optimization strategy for EAL loads

3.1. Autonomous PFR architecture for EAL loads

In this paper, a local PFR architecture for EAL loads is proposed, as illustrated in Fig. 2. The architecture integrates a PLC into the aluminum smelter, modifying the original current control system to enable local autonomous regulation.

The PLC acquires production parameters from the electrolytic cells and position data of the saturable reactors from the current control system. These data are used to optimize the PFR parameters, which are then transmitted back to the current control system.

In the proposed architecture, the actuator of PFR is the modified current control system. It continuously monitors the grid frequency through local sensors and adjusts the DC current according to the optimized PFR parameters, thereby enabling the load power to actively respond to frequency deviations in real time.

Further details regarding the PFR control scheme and the parameters optimization model are provided in the following sections.

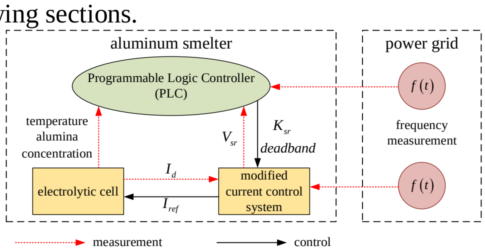

Fig. 2 Local PFR architecture for EAL loads.

3.2. Autonomous PFR control scheme for EAL loads

This paper investigates the PFR strategy of EAL load under the *Implementation Rules for the Management of Electricity Ancillary Services in the Southern Region* (hereinafter referred to as "Rules").

The "Rules" specify the performance indicators for directly controllable adjustable loads participating in PFR ancillary services, as summarized in Table 2.

By adjusting the DC current, the EAL can achieve continuous and precise power response with a time delay of less than 3s, satisfying the requirements for start-up time, response time, adjustment time and adjustment accuracy defined in the "Rules".

As shown in Fig.1, under normal operation, the EAL operates at nearly constant power. Minor voltage fluctuations are compensated by the current control system, while grid frequency fluctuations do not influence the active power. Therefore, to enable automatic and rapid response of the EAL to frequency deviations, this paper proposed a modification scheme for the original current control system.

The control block diagram of the transformed current control system is illustrated in Fig. 3. The area enclosed by the dashed box represents an additional frequency feedback control module, which consists of three functional components: a dead-zone unit, a linear-gain unit, and a limiting unit.

With the integration of the frequency feedback control module, the current control system is capable of automatically acquiring the grid frequency and computing the corresponding frequency deviation, which can be expressed as

$$\Delta f = f - f_N \tag{21}$$

$$\Delta f_d = \begin{cases} 0, & |\Delta f| \le \Delta f_{th} \\ \Delta f - \Delta f_{th}, & |\Delta f| > \Delta f_{th} \end{cases} \tag{22}$$

where Δf_{th} is the PFR deadband.

The additional reference current is:

$$\Delta I_{ref} = K_{sr} \Delta f_d \tag{23}$$

where K_{sr} is defined as the PFR feedback coefficient of EAL in this paper.

The power of EAL is:

$$P_f = (I_{ref,N} + \Delta I_{ref})^2 R + E(I_{ref,N} + \Delta I_{ref}) \tag{24}$$

Therefore, the electricity consumption of EAL is:

$$Q_P = \int_0^T P_f dt \tag{25}$$

The actual action integral electricity contributed is:

$$Q_f = \int_0^T |P_f - P_N| dt \tag{26}$$

According to the "Rules", the theoretical power of the load when participating in PFR is:

$$P_{fN} = P_N (1 + \Delta f_{dN} / f_N / K_N) \tag{27}$$

where K_N is the reference value of droop coefficient, 5%.

Based on the above analysis, the theoretical action integral electricity of the load can be calculated as follows.

Table 2
Performance indicators for directly controllable adjustable loads participating in PFR ancillary services [22]

indicators	value
frequency deadband	±0.05Hz (reference value)
droop coefficient $\frac{\Delta f}{f_N}\Big/\frac{\Delta P}{P_N}$	5% (reference value)
start-up time	⩽3s
response time	⩽12s
adjustment time	⩽30s
adjustment accuracy	⩽±2% of the adjustable load capacity

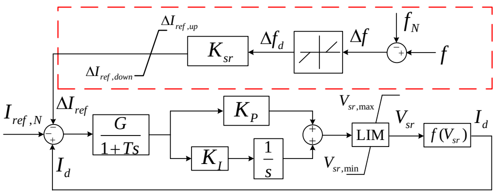

Fig. 3 Control block diagram of the transformed current control system.

$$Q_{fN} = \int_0^T \left|P_{fN} - P_N\right| dt \tag{28}$$

For loads that participate in PFR ancillary services and perform qualified regulation actions, the corresponding compensation amount is determined according to (29).

$$C_{comp} = \max\left((Q_f - 0.7Q_{fN}),0\right) \times 0.5 \times R_1 \tag{29}$$

where R_1 is the PFR compensation standard.

The design of the deadband and the PFR feedback coefficient directly influences the additional reference current and consequently, the action integral electricity. When the actual action integral electricity exceeds 70% of the theoretical action integral electricity, the PFR action is qualified and PFR compensation can be obtained. However, an economic trade-off emerges, as the ancillary revenue from PFR is gained at the expense of reduced electricity consumption and, consequently, lower production profit.

Beyond these economic considerations, participation in PFR also disrupts the electrolysis process. Aluminum smelting is engineered for steady-state, constant-current operation, with only minor fluctuations permitted around the rated value. In contrast, PFR induces frequent current variations, which alter the magnetic field in the cell and changes in the anode current density. These effects reduce production efficiency, increase the probability of anode effects, and ultimately threaten the stability and output efficiency of the electrolysis process. Because aluminum smelters differ in their tolerance to such disturbances, they inevitably make different trade-offs between economic incentives and operational stability.

Accordingly, this paper formulates a multi-objective optimization model that yields a set of optimal deadband and feedback coefficient solutions from which aluminum smelters can autonomously select according to operational preferences.

3.3. Proposed optimization model for PFR parameters

To provide aluminum plants with a set of PFR parameters that balance economic viability and production safety, a multi-objective optimization model is developed. This model aims to maximize net income from ancillary services while simultaneously minimizing the electrolysis process disturbance index. It accounts for both the multiphysics-based production safety constraints and grid-defined performance qualification requirements. Taking the grid frequency profiles and load production status as inputs, the model optimizes the frequency deadband and feedback coefficient. The resulting Pareto-optimal solution set provides a decision space, allowing aluminum plants to select PFR parameters that align with their specific risk-benefit preferences. The proposed multi-objective optimization model is formulated as follows.

$$\begin{cases} obj.1: MaxW \\ obj.2: Min\lambda \\ s.t.: Eq.(11),(20),(35) \end{cases} \tag{30}$$

where W is the net change in income before and after PFR, λ is the electrolysis process disturbance index.

(1) Proposed model objectives

1) Net income objectives

During the PFR process, the qualified PFR electricity yields ancillary service compensation revenue, whereas the reduction in total electricity consumption decreases aluminum output and consequently reduces production profit. Therefore, the net change in load income before and after PFR is expressed as

$$W = R - P \tag{31}$$

$$R = C_{comp} \tag{32}$$

$$P = \frac{Q_f}{W_{AL}} C_{AL} \tag{33}$$

where R denotes the compensation revenue from PFR ancillary services, P represents the production profits, W_{AL} denotes the electricity consumption per ton of aluminum, and C_{AL} is represents the profits per ton of aluminum.

2) Electrolysis process disturbance index objectives

We quantify the current fluctuation during PFR by integrating the squared first-order difference of the current over time. The electrolysis process disturbance index is then obtained by normalizing this metric with respect to its value under normal operating conditions.

$$\lambda = \int\left(\Delta I_f(t)\right)^2 \mathrm{d}t \Big/ \int\left(\Delta I_0(t)\right)^2 \mathrm{d}t \tag{34}$$

where I_f denotes the current during PFR, and I_0 represents the current under normal operation.

(2) Proposed model constraints

In addition to the multiphysics-based production safety constraints established in Section II, the optimization model must also satisfy the performance requirements defined by grid operational regulations. To ensure the effectiveness of the frequency response, the PFR action is considered qualified only when the ratio of the actual integral of regulated electricity to its theoretical value exceeds 70%, which is expressed as follows:

$$Q_f \geq 0.7Q_{fN} \tag{35}$$

3.4. Problem solution procedure

To solve the proposed multi-objective optimization model, this study employs the non-dominated sorting genetic algorithm II (NSGA-II). The algorithm yields the Pareto-optimal frontier, revealing the trade-off between net income and electrolysis process disturbance index, and provides a set of feasible solutions that satisfy production safety constraints, thereby enabling aluminum smelters to make decisions according to their respective preferences.

In addition, to provide an objective reference solution for aluminum smelters, this study employs the geometric knee-point decision method to identify the knee-point solution on the Pareto frontier. Beyond this point, any marginal improvement in one objective results in a significant deterioration in the other. Accordingly, the knee-point solution is adopted as the optimized solution for subsequent simulation analyses.

To address diverse frequency disturbance events, this paper proposes an *offline optimization–online matching* decision framework designed to rapidly identify PFR parameters for any given disturbance.

Using the N locally stored historical frequency events, the maximum rate of change of frequency (*RoCoF*) and the *final* frequency deviation within an initial time window (T_{window}=200 ms) are extracted to form the feature vector $\boldsymbol{V}_i$ for each event. For every event, the compensation standard and production safety boundaries are provided as inputs to generate the optimal PFR parameters set under the prevailing operating conditions. Depending on the decision-maker's preference—or alternatively, the knee-point-based selection method—the optimal parameters is chosen. This yields a strategy lookup table of the form {scenario i, $\boldsymbol{V}_i$, K_{sr} deadband}. When any of the external or internal conditions—including compensation standard, production status, decision preference, or newly observed frequency disturbances—change, the optimization process is re-executed and the lookup table is updated.

Online matching aims to rapidly and safely select a set of PFR parameters from the lookup table for the current frequency disturbance.

(1) When a disturbance occurs, the feature vector $\boldsymbol{V}_{real}$ is extracted within the initial time window.

(2) Borrowing the notion of "dominance'' from multi-objective optimization, a historical frequency event is considered "dominant" over the current event if its feature vector $\boldsymbol{V}_i$ is worse than $\boldsymbol{V}_{real}$ in all dimensions. All such dominant scenarios are identified from the historical frequency event set.

(3) Among the dominant scenarios, the one whose feature vector has the smallest Euclidean distance to $\boldsymbol{V}_{real}$ is selected. The corresponding PFR parameters are then applied to enable fast frequency response of the load.

4. Case Study

4.1. Simulation Setup

To verify the effectiveness of the proposed strategy, an IEEE 39 Bus Power System is implemented on the RTDS platform. To emulate the operational characteristics of a power system with a high penetration of renewable energy and an EAL load, the synchronous generators G5 and G8 in the original system are replaced by photovoltaic plants of equivalent capacity. Meanwhile, the static load connected to Bus 28 is substituted with the dynamic EAL load model developed in this study. The topology of the modified system is illustrated in Fig. 4. The electrical parameters and production parameters of the EAL load are listed in Table 3 and Table 4, respectively. The PFR compensation standard R_1 is set to 30,000 CNY/MWh [23]. To comprehensively evaluate the performance of the proposed strategy under diverse grid operation conditions, the system's renewable penetration level is modeled as a random variable following a normal distribution $\boldsymbol{N}(0.15,0.025^2)$, while the equivalent load damping coefficient is assumed to follow $\boldsymbol{N}(0.5,0.15^2)$. PFR events in the simulation are triggered by N-1 generator contingencies. Specifically, generators G3, G4, G6, G7, G9, G10 are considered potential outage units, each with an equal probability of failure.

In this simulation, the bath temperature fluctuation during PFR is limited to within ±0.5°C , and the deviation of the alumina content is constrained to within ±10% of rated value.

To improve solution efficiency while maintaining numerical accuracy, the frequency sampling interval of the current control system is set to 20 ms. According to the "Rules", the simulation time is configured as 60 s.

4.2. Simulation Results

To construct the proposed offline strategy lookup table, nine independent sample events are generated from the previously defined random scenario space to form a historical frequency event set, which emulates the historical frequency variations observed during actual load operation.

For each event in this historical set, a multi-objective optimization algorithm is executed to determine the corresponding optimal PFR parameters. The decision-variable search space is defined as follows: the PFR feedback coefficient ranges from [0, 200], and the deadband ranges from [0.02, 0.05] Hz.

The optimal strategy lookup table, presented in Table 5, is then obtained by extracting the knee-point solution from the Pareto frontier corresponding to each frequency event.

Taking the frequency event S5 as an example, the corresponding Pareto frontier set is illustrated in Fig. 5.

An examination of all optimal solutions along the Pareto frontier reveals that the PFR deadband remains consistently at 0.02 Hz across all test scenarios. This consistent pattern indicates that, rather than adjusting the deadband, the trade-off between net income and operational stability is predominantly governed by adjusting the PFR feedback coefficient, which thus serves as the primary control variable in achieving optimal performance.

As shown by point A on the Pareto frontier in Fig. 5, when the load adopts an extremely conservative solution, the compensation revenue from ancillary services is insufficient to offset the associated production costs, leading to a negative net benefit. This phenomenon defines the economic boundary of EAL participation in PFR.

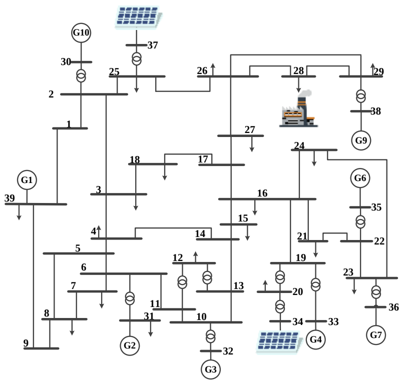

Fig. 4 Modified topology of the IEEE 39 Bus Power system.

Table 3
Electrical parameters of EAL

parameters	I_d (kA)	R (Ω)	E (kV)	V_{RE} (kV)	η
value	200	0.0045	0.13	0.45	94%

Table 4
Production parameters of EAL

parameters	W_{AL} (kWh/t)	C_{AL} (CNY/t)	C (J/g·°C)	h (W/m²·°C)	A (m²)
value	13500	5000	1.0178	800	12000

Table 5
Lookup table of offline-optimized PFR parameters

scenario	feature vector (max *RoCoF*, final frequency deviation)	feedback coefficient	deaband
S1	(-0.1822, -0.0375)	65.3513	0.02
S2	(-0.1825, -0.0395)	65.0083	0.02
S3	(-0.3883, -0.0803)	29.3499	0.02
S4	(-0.4897, -0.0965)	27.6145	0.02
S5	(-0.1830, -0.0389)	61.6768	0.02
S6	(-0.3426, -0.0703)	31.5926	0.02
S7	(-0.1827, -0.0395)	59.4983	0.02
S8	(-0.4964, -0.0980)	27.5400	0.02
S9	(-0.4728, -0.0867)	30.7495	0.02

To reveal the optimal parameters selection under different preferences, two representative solutions on the Pareto frontier were examined: a conservative solution and an aggressive solution. A risk-averse decision-maker would likely adopt the conservative strategy, in which the load employs a relatively small PFR feedback coefficient, achieving a net return of CNY 1.5 thousand while maintaining low operational disturbance. In contrast, a risk-seeking decision-maker may prefer the aggressive solution, characterized by a larger PFR feedback coefficient, to maximize PFR revenues.

In summary, the Pareto frontier analysis not only offers decision-makers a spectrum of optimal PFR parameters tailored to different preferences, but also identifies the key control parameters and delineates the economic boundaries of EAL participation in PFR. These findings provide valuable theoretical insights and practical guidance for engineering implementation.

As illustrated in Fig. 6, following a frequency disturbance, the current and power of EAL load respond rapidly and accurately to the dynamic variations in system frequency, thereby providing power support to the grid. This validates the effectiveness of the proposed PFR control scheme.

As shown in Fig. 7, both the bath temperature and the alumina content of the cell remain strictly within prescribed safe operating ranges, without violating any constraint boundaries.

4.3. Comparative Analysis

To evaluate the economic performance and operational safety of the proposed strategy, it is compared against a baseline strategy that adopts the reference PFR parameters specified in the "Rules". Simulation tests are conducted under two scenarios: 1) the historical frequency event S1, and 2) a randomly generated PFR event whose frequency characteristics fall within the envelope of historical observations. The performance of both strategies with respect to the optimization objectives and associated constraints is summarized in Table 6 and Table 7.

The results demonstrate that the proposed PFR parameter optimization method consistently maintains the operational disturbance at a similar level. When the frequency disturbance is mild, the optimized strategy responds more aggressively, enabling the load to secure higher economic returns. In contrast, when the disturbance is severe, the strategy deliberately reduces its response intensity to avoid elevated operational disturbance.

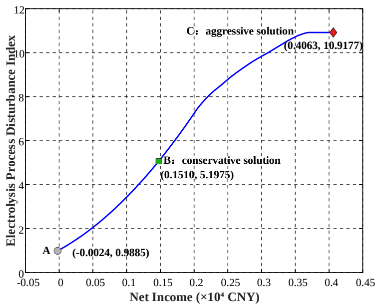

Fig. 5 Pareto frontier of net income and electrolysis process disturbance index for the EAL load.

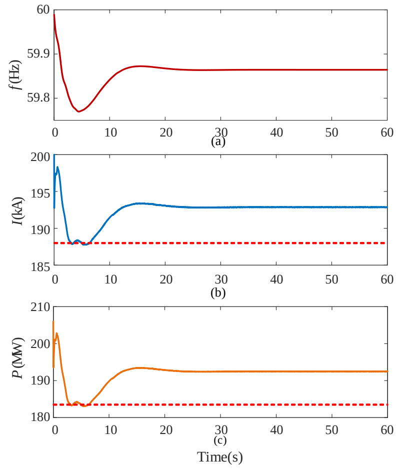

Fig. 6 The response curves in S5. (a) power grid frequency, (b) load DC current, (c) load power.

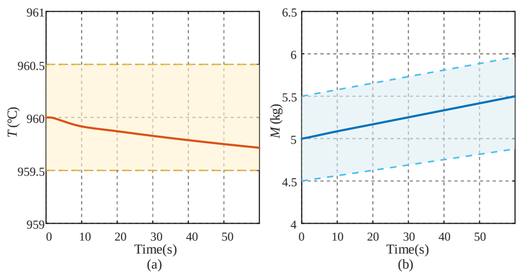

Fig. 7 Load production status curves in S5. (a) bath temperature, (b) alumina content.

The baseline strategy with fixed parameters, however, exhibits an inefficient and economically suboptimal response pattern. Because its control logic does not account for the load's preferences or production safety boundaries, it under-responds to mild disturbances, thereby reducing the net income from PFR. Under severe disturbances, it instead over-responds, leading to a sharp increase in operational disturbance and even the potential violation of production safety constraints.

The fundamental reason behind this difference is that the proposed framework treats the load as an autonomous decision-making agent that explicitly balances economic benefits against operational disturbance. Its objective in optimizing the PFR parameters is to maximize the attainable benefit subject to acceptable operational disturbance, rather than to pursue PFR performance at any cost. When a severe disturbance is detected, maintaining production safety naturally becomes the highest priority. In contrast, the reference parameters specified in the "Rules" neglect both the load's preferences and its intrinsic safety constraints.

Table 6

Performance comparison between the proposed and baseline strategies in scenario s1

	proposed strategy	baseline strategy
net income ($\times 10^4$ CNY)	0.2458	0.0427
electrolysis process disturbance index	8.0797	2.6797
constraint satisfied	yes	yes

Table 7

Performance comparison between the proposed and baseline strategies in the random scenario

	proposed strategy	baseline strategy
net income ($\times 10^4$ CNY)	0.0874	0.1306
electrolysis process disturbance index	8.4041	16.4236
constraint satisfied	yes	yes

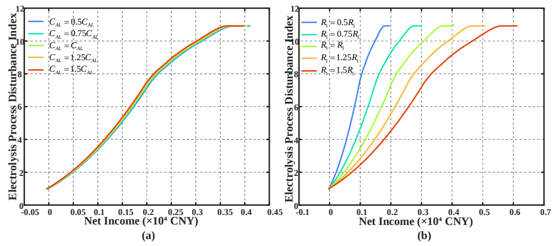

Fig. 8 Sensitivity analysis of economic parameters on the Pareto frontier. (a) effect of production profit parameter on the Pareto frontier. (b) effect of compensation standard on the Pareto frontier.

Accordingly, compared with the fixed parameter values prescribed by the grid, the optimization model developed in this paper enables loads to rationally trade off risk and benefit while safeguarding their own operating limits, thereby allowing them to participate in PFR in a more economical manner.

4.4. Sensitivity Analysis

To investigate the influence of external economic factors on load PFR decision-making, this section uses the frequency event S5 as the benchmark case. And the analysis focuses on the sensitivity of the production profit parameter and the compensation standard.

The reference values of these parameters are perturbed by ±25% and ±50%, respectively, and the Pareto frontiers corresponding to different economic parameter settings are obtained. The results are illustrated in Fig. 8.

As illustrated in Fig. 8(a), when the production profit increases, the Pareto frontier exhibits a slight shift toward the upper left, corresponding to a decrease in net income and a smoother electrolysis process. This behavior arises because, under the same disturbance index, a higher production profit amplifies the cost associated with power reduction during PFR, thereby suppressing the achievable net income.

In contrast, Fig. 8(b) shows that the influence of the compensation standard on PFR decisions is more pronounced. As the compensation standard increases, the Pareto frontier shifts markedly toward the lower right. This result suggests that greater economic compensation can effectively offset production losses, allowing the load to achieve improved profitability under the same disturbance index.

Overall, variations in the production profit and compensation standard alter the trade-off between the load's net income and disturbance index, thereby influencing its PFR behavior. Changes in the production profit parameter exert a relatively limited impact on the load's decision-making, whereas the compensation standard serves as the dominant factor determining the aggressiveness of frequency regulation. This is because the economic incentives provided by current market mechanisms substantially outweigh the cost variations caused by fluctuations in production profit.

These findings indicate that, from the perspective of aluminum smelter, PFR decisions are primarily driven by external market incentives rather than by internal production cost deviations. Consequently, the proposed strategy demonstrates strong practicality and robustness, as its effectiveness is less sensitive to uncertainties in internal cost estimation.

5. Conclusions

This paper develops an autonomous control and parameter optimization framework to support the practical participation of EAL loads in PFR ancillary services. By introducing local frequency measurement and feedback into the existing industrial current control system, the proposed framework enables EAL loads to respond autonomously to frequency deviations without relying on external regulation commands. To determine the feasible range of PFR operation, an electrical, thermal, and material coupled dynamic model is established, through which production safety constraints are quantitatively transformed into energy boundaries applicable to PFR control. On this basis, the frequency deadband and droop coefficient are optimized by simultaneously considering ancillary service revenue and production risk. The resulting Pareto optimal solutions provide flexible parameter choices for aluminum smelters with different operating requirements and risk preferences.

Simulation results demonstrate that the proposed framework enables EAL loads to provide rapid and accurate autonomous PFR while satisfying the derived production safety boundaries. The optimized control parameters effectively coordinate the economic benefits obtained from PFR ancillary services with the associated production risk, rather than simply maximizing the regulation response. These results indicate that the large regulation potential of EAL loads can be translated into practical ancillary service capability through appropriate local control and parameter configuration. The proposed approach therefore provides a feasible pathway for continuously operated industrial loads to participate in PFR as active flexible resources while preserving their original production functions.

Acknowledgments

This research is supported by the National Key Research and Development Program of China (No.2023YFB2407300).

References

[1] Koubar, M., Lindberg, O., Lingfors, D., Huang, P., Berg, M., Munkhammar, J., 2025. Techno-economical assessment of battery storage combined with large-scale photovoltaic power plants operating on energy and ancillary service markets. Appl. Energy 382, 125200.

[2] Zhao, T., Liu, H., Wang, N., Su, J., Luo, Z., Ma, S., 2025. An active power control of DFIG-based wind turbine generators for frequency regulation with expected dynamic performance. Appl. Energy 391, 125948.

[3] Liu, Z., Xie, J., Liu, Y., et al., 2023. Power demand-side flexibility series: Overview of flexibility potential in the electrolytic aluminum industry. Rocky Mountain Institute. Available at: https://rmi.org.cn/insights/industrial-dsf/ (accessed 30 June 2026).

[4] Yue, X., et al., 2024. Collaborative optimization of renewable energy power systems integrating electrolytic aluminum load regulation and thermal power deep peak shaving. Appl. Energy 373, 123869.

[5] National Bureau of Statistics of China, 2026. Statistical Communiqué of the People's Republic of China on the 2025 National Economic and Social Development. Available at: https://www.stats.gov.cn/sj/zxfb/202602/t20260228_1962662.html (accessed 30 June 2026).

[6] National Energy Administration of China, 2026. Electricity Consumption of the Whole Society Increased by 5.0% in 2025. Available at: https://www.nea.gov.cn/20260121/715f79826488476a9162da7c8bd77c80/c.html (accessed 30 June 2026).

[7] Chen, Y., Li, L., Li, W., Gao, S., Wang, X., Han, L., 2022. Research on electrolytic aluminum load participating in power grid stability control scheme, Power Demand Side Manage. 24, 21–27.

[8] Liao, S., Pi, S., Xu, J., Li, L., Ke, D., Sun, Y., 2025. Emergency control strategy for electrolytic aluminum load considering the load's transient overcurrent characteristics and transient voltage stability constraints. IEEE Trans. Power Syst. 40, 1699–1711.

[9] Liao, S., Xu, J., Sun, Y., et al, 2016. Load-damping characteristic control method in an isolated power system with industrial voltage-sensitive load. IEEE Trans. Power Syst. 31, 1118–1128.

[10] Liao, S., Xu, J., Sun, Y., Bao, Y., 2018. Local utilization of wind electricity in isolated power systems by employing coordinated control scheme of industrial energy-intensive load. Appl. Energy 217, 14–24.

[11] Liao, S., et al., 2022. Frequency stability control method for EAL participation in power grid considering the static voltage stability constraints. Proc. CSEE 42 (18), 6727–6740.

[12] Liao, S., Pi, S., Xu, J., Ke, D., Sun, Y., 2023. Review of key technologies for multi-level cooperative regulation of direct-controlled loads in new power systems. High Volt. Eng. 49 (9), 3669–3685.

[13] Obaidat, M., Al-Ghandoor, A., Phelan, P., Villalobos, R., Alkhalidi, A., 2018. Energy and exergy analyses of different aluminum reduction technologies. Sustainability 10, 1216.

[14] Nie, S., Huang, R., Chen, L., Ming, Y., You, G., Wu, C., 2024. Adaptive control of primary frequency regulation for EAL load considering energy recovery. Autom. Electr. Power Syst. 48 (17), 37 – 45.
[15] Liao, S., Bian, S., Xu, J., Ke, D., Sun, Y., 2025. Evaluation of grid-load interactive adjustable capacity of EAL load considering optimization of electrolytic cell energy flow. Proc. CSEE 45 (6), 2110 – 2121.
[16] Yi, J., Bai, J., Zhou, W., He, H., Yao, L., 2018. Operating Parameters Optimization for the Aluminum Electrolysis Process Using an Improved Quantum-Behaved Particle Swarm Algorithm. IEEE Transactions on Industrial Informatics 14, 3405–3415.
[17] Jiang J. Study on the control of alumina concentration for large-scale industrial aluminum reduction cells [MS thesis]. Shenyang (China): Northeastern University; 2017.
[18] Shi, J., Yao, Y., Bao, J., Skyllas-Kazacos, M., Welch, B.J., Jassim, A., Mahmoud, M., 2022. Advanced Model-Based Estimation and Control of Alumina Concentration in an Aluminum Reduction Cell. JOM 74, 706–717.
[19] Taylor, M.P., Chen, J.J.J., 2015. Technique for Low Amperage Potline Operation for Electricity Grid Storage. Metallurgical and Materials Transactions E 2, 87–98.
[20] Qiu Z. Aluminum smelting with prebaked anodes. 3rd ed. Beijing (China): Metallurgical Industry Press; 2005.
[21] Bao P. Coordinated active power/frequency control from supply, network, and demand sides considering participation of aluminum smelter load [MS thesis]. Jinan (China): Shandong University; 2021.
[22] South China Energy Regulatory Bureau of National Energy Administration of the People's Republic of China. Notice on the issuance of the "Implementation Rules for the Management of Electricity Grid Connection Operation in the Southern Region" and the "Implementation Rules for the Management of Electricity Ancillary Services in the Southern Region". https://nfj.nea.gov.cn/xxgk/fdzdgknr/scjg/202402/t20240208_240258.html [accessed 15 June 2026].
[23] South China Energy Regulatory Bureau of National Energy Administration of the People's Republic of China. Notice on the issuance of the "Major Revised Articles of the 'Two Detailed Rules' of the Southern Region". https://nfj.nea.gov.cn/xwzx/tzgg/202412/t20241218_274102.html [accessed 15 June 2026].